

region (21, 23). The epicontinental climate system is characterized by seasonal alterations of the East Asian summer and winter monsoons (24).

The ECS receives massive amounts of terrestrial sediments [about 2×10^9 tons/y (a)] transported by the Yangtze River and other rivers from the surrounding regions (25). During the Last Glacial Maximum (LGM), the ECS sea level was at least 125 m lower than at present; thus, most of the present shelf was exposed (22). The Okinawa Trough, close to the ECS shelf edge, has a water depth of more than 2,700 m in places and was continuously submerged during the glacial/interglacial cycles; thus, it continuously accumulated deposits of mixed terrestrial and marine sources.

Core DG9603 was taken from the mid-Okinawa Trough (28° 08.869'N, 127°16.238'E, water depth of 1,100 m) (Fig. 1). This 5.85-m core has continuous accumulation of semipelagic abyssal ooze with abundant microfossils, and the age model was established using accelerator mass spectrometry (AMS) ^{14}C dates (17, 18). Twelve samples for AMS ^{14}C dating were obtained from monospecific samples of the planktonic foraminifera *Globorotalia menardii*, *Globigerinoides sacculifer*, and *Neogloboquadrina dutertrei* (Table S1). The ^{14}C ages were converted to calendar ages using software CALIB 6.1 (26) and Marine09 datasets (27). The ages of samples from bottom to top were estimated by linear interpolation of these age control points. The top 4.5 m covers the past 42 ka, with an average resolution of ca. 208 a per sample.

Results

Vegetation Changes in Epicontinental Areas of the ECS. The relative abundance of subtropical evergreen arboreal taxa [*Quercus E* (evergreen) and *Castanopsis-Lithocarpus*], temperate arboreal taxa [*Quercus D* (deciduous)], and herbaceous species (Cyperaceae and *Artemisia*) revealed large (ca. 20–40%) and abrupt changes ca. 26.5 kaBP and ca. 15 kaBP (Fig. 2 and Figs. S1 and S2). Their absolute concentrations display similar changes (Fig. S3).

From ca. 26.5–15 kaBP, *Quercus D* rapidly increased, whereas *Quercus E* and *Castanopsis-Lithocarpus* significantly decreased. The maximum values of steppe and wetland taxa (*Artemisia* and Cyperaceae) and minimum values of the first principal component

(F1) of principal components analysis (PCA) (Methods) indicate that the coldest climate occurred in this period during the past 40 ka. After ca. 15 kaBP, the sharp increase of tropical/subtropical evergreen arboreal taxa (i.e., *Quercus E*, *Castanopsis-Lithocarpus*), with a simultaneous decrease of *Quercus D* and herbaceous taxa, reflected a dramatic rise in temperature. Its timing coincided with an abrupt cold/warm and dry/wet transition observed in the Chinese cave stalagmites (29, 30) and in a Greenland ice core (31). A small increase in *Quercus D* and a slight decrease in *Quercus E* and *Castanopsis-Lithocarpus* during the interval from ca. 12.9–11.5 kaBP indicated a minor temperature reversal. The timing of this reversal corresponded with the cold Younger Dryas (YD) event. Notably, this temporal pattern of climate changes is similar to the last deglacial climate oscillation in the Greenland ice core (31) (Fig. 2).

Pollen in modern marine sediments of the ECS is derived from epicontinental vegetation along the adjacent eastern margin of China (32), from which location it is transported by rivers, winds, and long-shore currents and deposited in the ECS (33). Moreover, the exposed ECS shelf was also a major pollen source for the Okinawa Trough during the LGM and deglacial periods (32–34). Previous pollen records from the middle Okinawa Trough indicated that abrupt vegetation changes and land temperature increases were synchronous with the Bølling warm period warming observed in the Greenland ice core ca. 14.6 kaBP (34). Our evidence also corroborates this synchronous deglacial warming in the epicontinental climate of the ECS and northern high latitudes.

Asynchronous Marine and Terrestrial Signals During the Last Deglaciation. The high-resolution alkenone-based sea surface temperature (SST) (19, 20) record shows that a continual deglacial warming began around 20–19 kaBP, starting from the coldest estimated SST of 21 °C (i.e., about 5–6 °C lower than the modern SST; Fig. 3F). Similarly, the winter sea surface temperature (SSTw) reconstructed from fossil foraminiferal data of the same site using foraminiferal transfer functions (17, 18) yielded a comparable pattern for the last deglacial warming that started ca. 20–19 kaBP (Fig. 3G).

In both records, SSTw and U^{k}_{37} SST estimates had similar trends during the transition from the late glacial to the Holocene. However, the SSTw curve showed a relatively larger amplitude of SSTw variation than U^{k}_{37} SST, because the foraminiferal transfer function has a higher sensitivity than alkenone methodologies (5). Notably, the pattern of this transition was similar to that of the last deglacial warming recorded in marine core from the Western Pacific Warm Pool (WPWP) (35) (Fig. 3H), suggesting a direct link in SST changes between the Okinawa Trough and the tropical Pacific.

they avoid the pitfall of age uncertainties arising from correlations of proxy records obtained from different cores with different radiocarbon dating controls. The timing of oceanographic changes in the ECS significantly led the corresponding variations in its epicontinental vegetation and climate by about 3–4 ka on glacial/interglacial time scales (Fig. 3).

Discussion and Conclusions

Vegetation Changes and the East Asian Monsoon. The East Asian monsoon is a dynamic, interactive climate system driven by two seasonally reversing mechanisms. In summer, the differential heating produces an atmospheric pressure gradient between an ocean and continent that forces a steady flow of warm and moist maritime air onto the continent (i.e., the East Asian summer monsoon). In winter, the atmospheric pressure gradient is reversed, resulting in the flow of cold, dry air out from north-central Asia (i.e., the winter monsoon). Vegetation changes on the East Asian continent are mainly controlled by these two monsoon seasons (33, 34). Because the plant community response to climate changes is very rapid, probably within a few decades (38, 39), a high-resolution pollen record derived from core DG9603 revealed not only vegetation but Asian monsoon changes in epicontinental areas of the ECS.

From ca. 40–26.5 kaBP, these areas were covered by warm temperate forest-steppe and wetlands, indicating a relatively strong summer monsoon. During the period of ~26.5–15 kaBP, wetland and temperate steppe (or a mosaic of forest and grassland) developed, reflecting a stronger winter monsoon. In this period, a gradual reduction of *Artemisia* occurred from ca. 18–15 kaBP. As shown in Fig. 2 and Fig. S2, *Artemisia* pollen was mainly replaced during this period by Cyperaceae and *Quercus D*, which have ecological and climatic implications relative to *Artemisia* in the pollen record, suggesting no major change in epicontinental vegetation types and climate before and after 18 kaBP. This gradual

reduction of *Artemisia* might be ascribed to the shrinking of the grass-covered ECS continental shelf due to the rise of the deglacial sea level (33, 34) rather than to climate change. The exposed continental shelf was composed mainly of saline sandy soil favorable to the growth of *Artemisia* (40); thus, the gradual decrease of *Artemisia* in deglacial sediments likely reflected the process of marine transgression on the previously exposed shelf (34, 40). It is

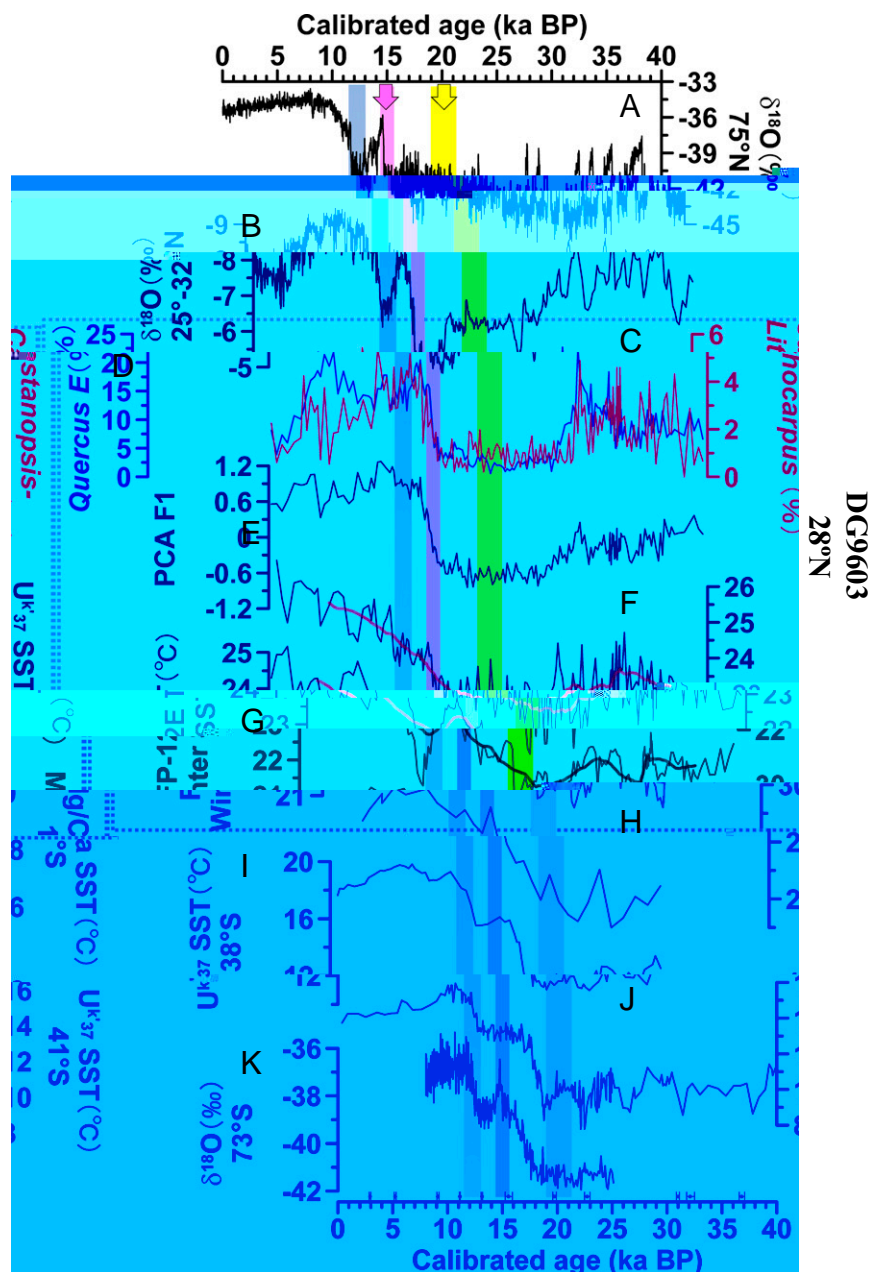


Fig. 3. Comparison of deglacial climate proxy records from core DG9603 with other proxy records for temperature and circulation in the Antarctic Ocean, Pacific Ocean, Greenland, and East Asia. $\delta^{18}\text{O}$ record from the NGRIP (31) [on a GICC05 time scale (28)], $\delta^{18}\text{O}$ records from Hulu and Dongge caves (29, 30) (B), multiproxy records of core DG9603 in the dashed blue box [*Castanopsis-Lithocarpus* (C), *Quercus E* (D), PCA F1 (E), U^{k}_{37} SST (19, 20) (F), and FP-12E SSTw (18) (G)], Mg/Ca SST in MD97-2138 core (35) (H), U^{k}_{37} SST in MD03-2611 core (36) (I), U^{k}_{37} SST in ODP1233 core (37) (J), and $\delta^{18}\text{O}$ record from Taldice (on a GICC05 time scale) (12) (K). Black dots at the bottom indicate dating control points with 1σ uncertainty for the DG9603 core. The yellow-shaded bar (arrow) and pink-shaded bar (arrow) show the timing of the last deglacial warming in SST records from the WPWP (H) and ECS (F and G), and in terrestrial climate records from East Asia (B–D) and Greenland (A), respectively; the blue-shaded bar shows the YD cold period. Red lines in F and G are 25-point running averages.

Okinawa Trough also displayed a continuous deglacial warming pattern beginning at *ca.* 19 kaBP (42).

Understanding the cause of the continuous deglacial SST warming of the Kuroshio region that started *ca.* 20–19 kaBP offers important insights into the mechanisms for a linkage between the ECS and the tropical Pacific Ocean. The $\delta^{13}\text{C}$ record of planktonic foraminifera from the Kuroshio region showed a broad minimum during the last deglaciation in the Okinawa Trough (43). This event was consistent with the last deglacial $\delta^{13}\text{C}$ minimum in records from the western equatorial Pacific Ocean, which suggests that the source water may have come from the tropical Pacific Ocean during the last deglaciation (43). Because the last deglacial $\delta^{13}\text{C}$ minimum in records from the western equatorial Pacific Ocean was an important regional paleoceanographic event (43), the consistency in the timing of this event between two regions implies that signals from the tropical zone of the ocean can be rapidly delivered to the northern middle latitudes along the path of the Kuroshio region. It also suggests that warming

water evolution in the tropical Pacific Ocean played a key role in regulating SST variations of the ECS (43, 44).

A comparison of our SST records with those in the SCS showed that SST in the Okinawa Trough was influenced more significantly by SST changes in the tropical Pacific Ocean during the last deglaciation. The SCS, consisting of semienclosed marginal basins, was unlikely to be affected by Pacific Ocean open circulation, especially in the glacial period with a low sea level (6). It was more vulnerable to being influenced by the East Asian monsoon associated with high-latitude atmospheric circulation (45, 46).

Asynchronous Marine and Terrestrial Signals Associated with Low- and High-Latitude Climate Changes.

Low-latitude tropical regions (*ca.* 23°N–23°S) receive about half of the solar energy on the Earth’s surface (47, 48); the tropical ocean is therefore considered as the “heat engine” driving the global climate system on seasonal to geological time scales (49). However, what mechanisms caused the last deglacial warming that started at *ca.* 20–19

kaBP in the WPWP and its spreading from low-latitude oceans to high-latitude northern and southern oceans?

Shiau and Chen (46) found that the SST warming in the tropical regions at *ca.* 20–19 kaBP was synchronous with the increase of June local solar radiation at *ca.* 20 kaBP. This correspondence with the precessional cycle suggests that insolation could be the main factor responsible for early SST warming (46). De Deckker et al. (1) recently proposed another mechanism: An early phase of the last deglacial warming in the WPWP probably resulted from maximum austral summer insolation peaking at 21 kaBP (1), which stored a large amount of heat in the WPWP.

However, the heat storage in the WPWP may also be affected by other factors, especially the trade winds (47, 49, 50). Under the trade wind stress, the thermocline is deep in the West and shallow in the East; thus, a huge amount of heat is stored in the tropical western Pacific Ocean by the westward warm equatorial current, creating the WPWP. Geological records (51) and model simulations (52) revealed that SST increase in the WPWP was consistent with the strengthened intensity of trade winds, as the summer (June, July, August) solar radiation increased from 20 kaBP under the precessional cycle (47, 50–52). Therefore, the last deglacial warming beginning as early as *ca.* 20 kaBP in the WPWP was mainly driven by the tropical insolation and trade wind intensity (46, 52, 53).

With an excess of heat stored in the WPWP *ca.* 20 kaBP, the heat would have been transferred from low to high latitudes by the assistance of surface ocean currents. In the north of the WPWP, the warming water was moved northward by the Kuroshio Current to enter the ECS. This process led to the ECS warming *ca.* 20–19 kaBP, at the same time as in the WPWP. On the southern margin of the WPWP, the southward shift of the subtropical front and the rise in sea level allowed the stored heat in the WPWP to flow into the central Indian Ocean and then to escape into the Atlantic Ocean via the Agulhas Current, as De Deckker et al. (1) have proposed. The huge influx of warm saltwater into the Atlantic Ocean may have ultimately helped ton

ACKNOWLEDGMENTS. We thank the editor and two anonymous reviewers for several insightful comments that significantly improved the paper, Kam Biu Liu (Department of Oceanography and Coastal Sciences, Louisiana State University) for invaluable assistance, Patrick Rioual (Institute of Geology and Geophysics, Chinese Academy of Sciences) for significant advice, and John Anderson (Loughborough University) for assistance with language corrections. This study was supported by the National Natural

Science Foundation of China (NSFC) (Grants 41071131), the National Basic Research Program of China (973 Program) (Grant 2010CB950201), NSFC (Grants 41101183 and 41230104), and the Strategic Priority Research Program: Climate Change, Carbon Budget and Relevant Issues (XDA05130600). The materials used in this study were collected during the "Donghai" (ECS) cruise of *I/Atalante* in 1996, under the framework of the Chinese-French Cooperation in Oceanography study.

1. De Deckker P, Moros M, Perner K, Jansen E (2012) Influence of the tropics and southern westerlies on glacial interhemispheric asymmetry. *Nat Geosci* 5(4): 266–269.
2. Jennerjahn TC, et al. (2004) Asynchronous terrestrial and marine signals of climate change during Heinrich events. *Science* 306(5705):2236–2239.
3. Barker S, et al. (2009) Interhemispheric Atlantic seesaw response during the last deglaciation. *Nature* 457(7233):1097–1102.
4. Clark PU, et al. (2009) The Last Glacial Maximum. *Science* 325(5941):710–714.
5. Kiefer T, Kienast M (2005) Patterns of deglacial warming in the Pacific Ocean: A review with emphasis on the time interval of Heinrich event 1. *Quat Sci Rev* 24(7–9): 1063–1081.
6. Kienast M, Steinke S, Statterger K, Calvert SE (2001) Synchronous tropical South China Sea SST change and Greenland warming during deglaciation. *Science* 291(5511):2132–2134.
7. Castañeda IS, et al. (2010) Millennial-scale sea surface temperature changes in the eastern Mediterranean (Nile River Delta region) over the last 27,000 years. *Paleoceanography* 25(1):PA1208.
8. Benson L, Burdett J, Lund S, Kashgarian M, Mensing S (1997) Nearly synchronous climate change in the Northern Hemisphere during the last glacial termination. *Nature* 388(6639):263–265.
9. Clark PU, et al. (2012) Global climate evolution during the last deglaciation. *Proc Natl Acad Sci USA* 109(19):E1134–E1142.
10. Denton GH, et al. (2010) The last glacial termination. *Science* 328(5986):1652–1656.
11. Pedro JB, et al. (2011) The last deglaciation: Timing the bipolar seesaw. *Clim Past* 7(2): 671–683.
12. Stenni B, et al. (2011) Expression of the bipolar see-saw in Antarctic climate records during the last deglaciation. *Nat Geosci* 4(1):46–49.
13. Stocker TF, Johnsen SJ (2003) A minimum thermodynamic model for the bipolar seesaw. *Paleoceanography* 18(4):1087.
14. Shakun JD, et al. (2012) Global warming preceded by increasing carbon dioxide concentrations during the last deglaciation. *Nature* 484(7392):49–54.
15. Lea DW, Pak DK, Spero HJ (2000) Climate impact of late quaternary equatorial Pacific sea surface temperature variations. *Science* 289(5485):1719–1724.
16. Lu HY, et al. (2002) Asynchrony of the marine and epicontinental climate records in the East Asia during the last 20 ka. *Mar Geol Quat Geol* 22(1):17–23.
17. Li TG, et al. (2001) Heinrich event imprints in the Okinawa Trough: Evidence from oxygen isotope and planktonic foraminifera. *Palaeogeogr Palaeoclimatol Palaeoecol* 176(1–4):133–146.
18. Liu ZX, et al. (2001) The paleoclimatic events and cause in the Okinawa Trough during 50 kaBP. *Chin Sci Bull* 46(2):153–157.
19. Meng XW, Du DW, Liu YG, Liu ZX (2002) Molecular biomarker record of paleoceanographic environment in the East China Sea during the last 35,000 years. *Science in China Series D Earth Science* 45(2):184–192.
20. Xiong YQ, Liu ZX (2004) Variations in sediment provenance and its implications of Core DGKS9603 since the late Quaternary. *Acta Oceanol Sin* 26(2):61–71.
21. Wang PX (1985) *Marine Micropaleontology of China* (China Ocean Press, Beijing).
22. Saito Y, et al. (1998) Transgressive and highstand systems tracts and post-glacial transgression, the East China Sea. *Sediment Geol* 122(1–4):217–232.
23. Zhao B, Fang G (1991) The estimation of the flow of main waterways in the East China Sea. *Acta Oceanol Sin* 13(2):169–177.
24. Yancheva G, et al. (2007) Influence of the intertropical convergence zone on the East Asian monsoon. *Nature* 445(7123):74–77.
25. Hu D, Saito Y, Kempe S (1998) Sediment and nutrient transport to the coastal zone. *Asian Change in the Context of Global Climate Change: Impact of Natural and Anthropogenic Changes in Asia on Global Biogeochemical Cycles*, eds Galloway JN, Melillo JM (Cambridge Univ Press, Cambridge, UK), pp 245–270.
26. Stuiver M, et al. (1998) INTCAL98 radiocarbon age calibration, 24,000–0 cal BP. *Radiocarbon* 40(3):1041–1083.
27. Reimer PJ, et al. (2009) IntCal09 and Marine09 radiocarbon age calibration curves, 0–50,000 years cal BP. *Radiocarbon* 51(4):1111–1150.
28. Andersen KK, et al. (2006) The Greenland Ice Core Chronology 2005, 15–42 ka. Part 1: Constructing the time scale. *Quat Sci Rev* 25(23–24):3246–3257.
29. Wang YJ, et al. (2001) A high-resolution absolute-dated late Pleistocene Monsoon record from Hulu Cave, China. *Science* 294(5550):2345–2348.
30. Dykoski C, et al. (2005) A high-resolution, absolute-dated Holocene and deglacial Asian monsoon record from Dongge Cave, China. *Earth Planet Sci Lett* 233(1–2): 71–86.
31. Andersen KK, et al.; North Greenland Ice Core Project members (2004) High-resolution record of Northern Hemisphere climate extending into the last interglacial period. *Nature* 431(7005):147–151.
32. Xu D, Lu H, Wu N, Liu Z (2010) 30,000-Year vegetation and climate change around the East China Sea shelf inferred from a high-resolution pollen record. *Quat Int* 227(1):53–60.
33. Wang KF, Sun YH, Zhang YL, Jiang H, Zhang YC (1987) *The Spore-Pollen and Algal Assemblage in the East China Sea Sediments* (China Ocean Press, Beijing).
34. Zheng Z, et al. (2011) Pollen record of the past 60 ka BP in the Middle Okinawa Trough: Terrestrial provenance and reconstruction of the paleoenvironment. *Palaeogeogr Palaeoclimatol Palaeoecol* 307(1–4):285–300.
35. de Garidel-Thoron T, et al. (2007) A multiproxy assessment of the western equatorial Pacific hydrography during the last 30 kyr. *Paleoceanography* 22(3): PA3204.
36. Calvo E, Pelejero C, De Deckker P, Logan GA (2007) Antarctic deglacial pattern in a 30 kyr record of sea surface temperature offshore South Australia. *Geophys Res Lett*

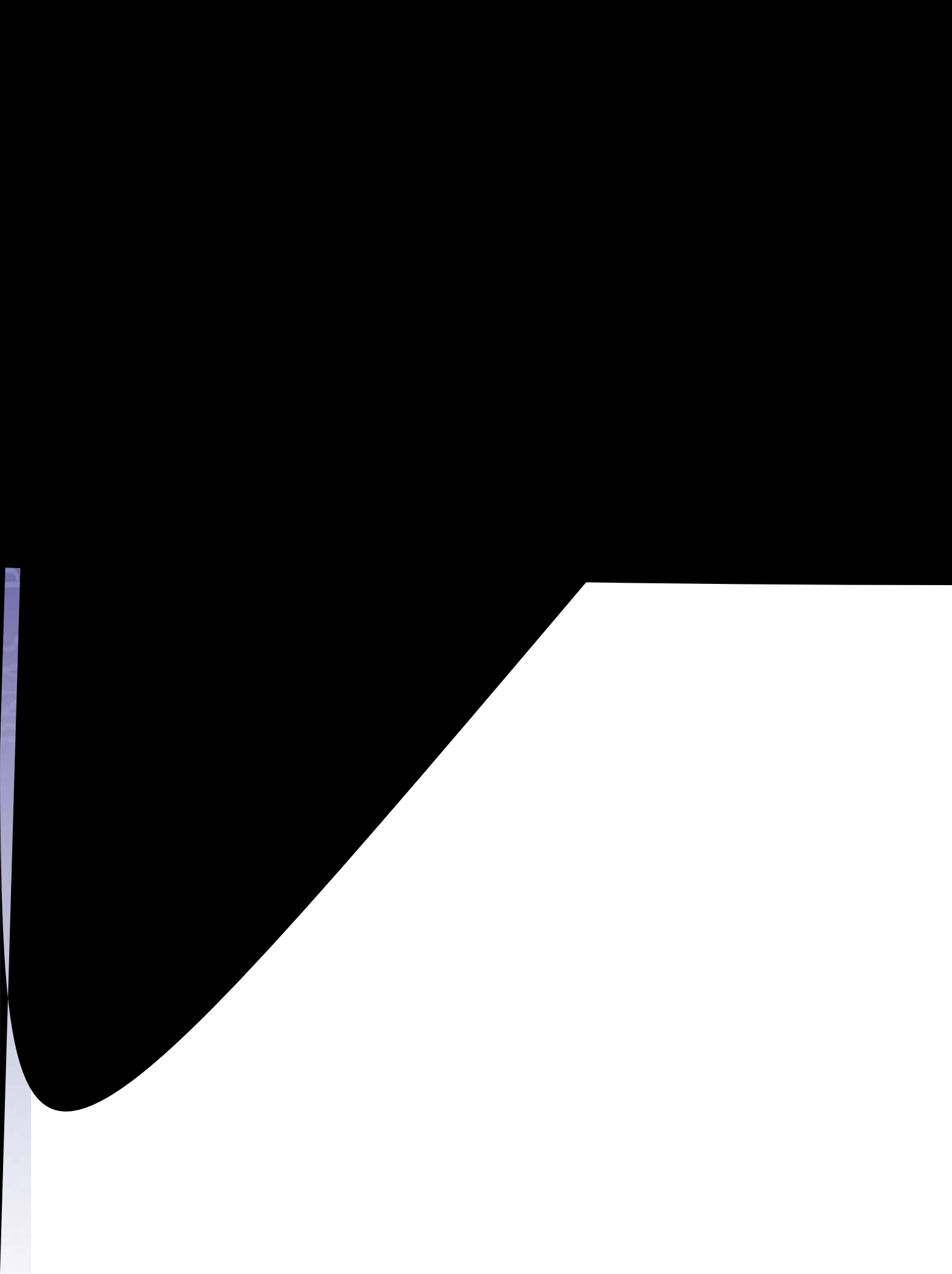


Table S2. Data of pollen (%), foraminifera transfer function (FP-12E), and alkenone paleothermometry ($U^{k'_{37}}$) proxies from core DG9603

[Table S2](#)

Table S3. Data of pollen counts from core DG9603

[Table S3](#)